

AN EVALUATION OF THE MECHANICAL BEHAVIOR OF BRONZE-NI COMPOSITES PRODUCED BY SELECTIVE LASER SINTERING

Mukesh K. Agarwala, David L. Bourell, Benny Wu, and Joseph J. Beaman.
Center for Materials Science and Engineering, and Department of Mechanical Engineering.
The University of Texas at Austin, Austin, Texas 78712.

ABSTRACT

Mechanical properties of Bronze-Nickel composites produced by Selective Laser Sintering (SLS) were evaluated by constant displacement tension tests. These were studied as a function of SLS process parameters - laser power density, scan speed, scan spacing, scan direction and layer thickness. The strength data was then correlated to the microstructure and the part bulk density. To further enhance the part densities and the mechanical properties, post-SLS sintering was studied. The relationships between SLS process parameters, post-SLS sintering parameters and the resulting microstructures, part bulk density and the mechanical properties will be described.

INTRODUCTION

Markets for rapid prototyping continue to grow as the demand for functional parts and prototype tooling increases. Several novel approaches exist to meet this demand. In recent years, Selective Laser Sintering (SLS) has emerged as one such process which can, not only produce parts from polymers successfully, but also is capable of producing parts from high temperature materials like metals and ceramics directly, without the aid of any low temperature binders (1,2).

Direct SLS of metals is extremely desirable as it avoids the time consuming and often tedious step of binder removal associated with indirect fabrication of metals and ceramics parts. This makes the production of prototype patterns, molds and dies for casting and injection molding, fast and economical.

However, any structural part produced, either by direct SLS or any other technique, is of little consequence unless it has the structural integrity to withstand the complex loading conditions that its use may require. In this study, the mechanical behavior of direct SLS Bronze-Nickel parts were evaluated, as this alloy system is being developed for use as molds in injection molding.

EXPERIMENTAL PROCEDURE

Sub-size tension test bars of Bronze-Nickel were made in the high-temperature SLS workstation developed at The University of Texas at Austin (3,4). The dimensions and geometry of the bars used in this study is shown schematically in Figure 1., which conforms closely with the ASTM Standard E8 (5) and the standard MPIF tension test bars for powder metallurgy materials (6).

Prealloyed, 90 Wt.% Cu - 10 Wt.% Sn, Bronze powders of particle size 30-50 μm and Ni powders of particle size 75-150 μm were mixed and SLS processed at laser powers of 35 W, 45 W, and 56 W with beam diameters of 0.875 mm, 1.06 mm, and 1.224 mm, respectively. Scan speeds in the range 0.2 to 1.5 inch/second were used. Layer thickness and scan spacing were kept constant at 0.01 and 0.02 inch, respectively. Scanning was done along the transverse and longitudinal directions of bars and layers were built in the thickness direction.

Post-SLS sintering was done for a series of tension test bars processed at 56 W laser power and scan speeds of 0.3"/sec. and 1.5"/sec. Post-SLS sintering of the bars was done at temperatures ranging from 900°C to 1100°C in flowing hydrogen for time periods varying from 1 to 10 hours. All tension testings were done in a constant displacement testing machine at a crosshead speed of 1 mm/min. Densities were measured by direct volume measurement. Phase

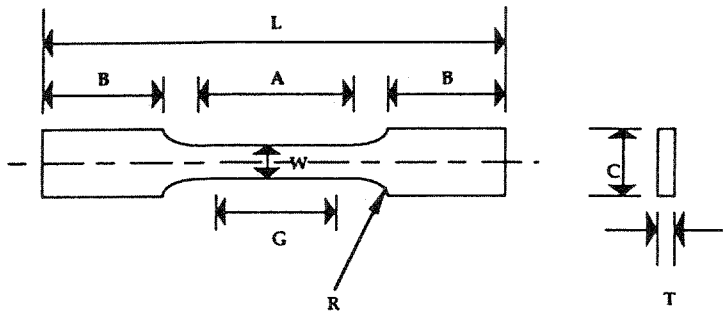


Figure 1. A Schematic of Tensile Bar Geometry Used to Make SLS Bronze-Ni Samples. ($L=3''$, $B=0.7''$, $A=1''$, $G=0.75''$, $W=0.2''$, $C=0.5''$, $R=0.375''$, and $T=0.25''$)

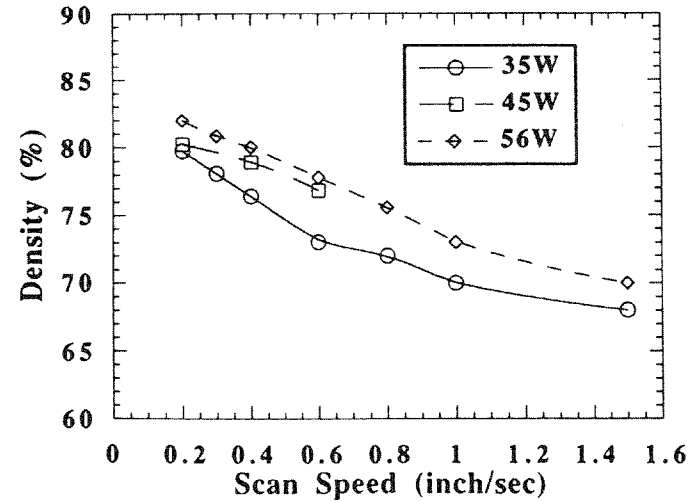


Figure 2. Fractional Density of SLS Bronze-Ni Parts as a Function of Scan Speed and Laser Power.

194

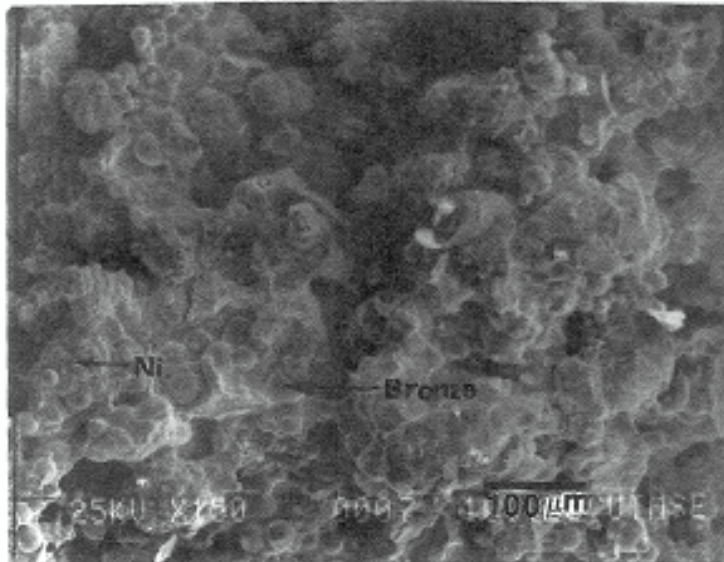


Figure 3. SEM of Fracture Surface of SLS Bronze-Ni Part Showing Melting of Bronze With No Melting of Ni.

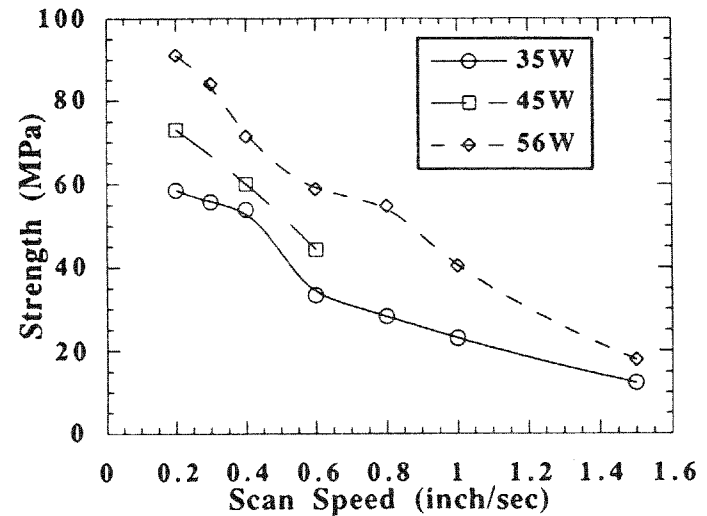


Figure 4. Tensile Strength of SLS Bronze-Ni Parts as a Function of Scan Speed and Laser Power.

analysis and microstructural analysis of the material was done at every step of processing by X-ray diffraction, optical microscopy, EDS and SEM.

RESULTS AND DISCUSSION

Preliminary experiments were done to investigate the effect of scan direction and layer thickness. From these experiments it was found that strengths were considerably lower when scanned in the longitudinal direction when compared to transverse direction. This is due to a better sintered part when the scan vector is short. Nelson, et al (7) have shown that a series of short scan vectors would receive more net energy than a series of longer scan vectors because of less delay between successive pulses.

As expected, lowering the layer thickness from 0.02" to 0.01" resulted in higher strength. However, on further lowering the layer thickness to 0.005" resulted in difficulty in spreading fresh layers without disturbing the previously sintered layers. This is especially the case during the early build-up of the part. Therefore, all further experiments were done at a constant layer thickness of 0.01" and all scanning was done along the short-transverse direction.

EFFECT OF SCAN SPEED AND LASER POWER

As shown in Figure 2, for a given laser power, density of the SLS Bronze-Nickel parts increased as the scan speed decreases. Also, the density is found to increase with increasing laser power, at a constant scan speed. Higher density is achieved with slower scan speed and higher laser power due to an increased amount of energy input to the powder surface. A higher amount of energy to the powders increases the temperature high enough to result in a larger amount of liquid phase formation. Bronze, which melts incongruently between 870°C (solidus) and 1030°C (liquidus), exhibits a higher degree of liquid formation as the temperature above the solidus increases. Also, as temperature increases, the viscosity of molten bronze decreases, facilitating more efficient densification with the solid nickel particles. An increase in temperature also lowers the wetting angle between liquid bronze and solid nickel to result in better wetting characteristics and improved densification. Figure 3 shows the fracture surface of a typical Bronze-Nickel part showing melting of bronze particles while the nickel particles are present without any significant melting. However, at very high laser powers and slow scan speeds (0.2"/sec. - 0.8"/sec.), significant amount of "curling" phenomenon was observed in the parts, as observed by Zong et.al. also (1). Experiments with varying bed temperatures showed that "curling" can be minimised by using high bed temperatures while keeping laser power high enough with slow scan speeds necessary for high density parts. However, at bed temperatures above 450°C, the entire powder bed undergoes light sintering and forms a "cake" around the SLS part. This makes it difficult to remove the SLS parts from the surrounding powder bed. Therefore, all experiments in this study were done at a bed temperature of 450°C.

Strength, which is primarily a function of fractional density (or porosity) (8), exhibited a similar trend as density with respect to scan speed and laser power, Figure 4. Pores reduce the effective load carrying capacity of a material. Also, pores act as stress concentrators and as effective crack initiation sites. Therefore, a sample with density less than 100% is expected to have a strength less than that of a fully dense wrought material. In addition to fractional density, the strength of such porous compacts depends on various powder characteristics such as particle size, particle size distribution and particle shape. The strength of porous compacts is expected to vary with fractional density ρ of the compact as follows :

$$\sigma = C \sigma_0 f(\rho) \quad (I)$$

where σ is the strength of compact, σ_0 is the wrought strength and $f(\rho)$ is a fractional density dependence function. Several studies have attempted to correlate strength with ρ by various forms of $f(\rho)$. The most commonly used relationship is of the form :

$$\sigma = C \sigma_0 \rho^m \quad (\text{II})$$

where C and m are empirical material constants and ρ is the fractional density.

POST-SLS PROCESSING OF BRONZE-NICKEL PARTS

In an attempt to further densify and hence improve strength, the SLS Bronze-Nickel tensile coupons were further processed by Liquid Phase Sintering (LPS) in hydrogen above the solidus temperature (870°C) of bronze. Before looking at the results of post-SLS processing, it is important to review the basic concepts of LPS (9) to better understand the results, especially with respect to Bronze-Nickel system. Liquid phase sintering in Bronze-Nickel system occurs in three stages :

STAGE I : At temperatures above the solidus temperature 870°C, bronze melts partially and above the liquidus 1030°C it melts completely. In this stage of LPS, the liquid bronze flows into the pores and a rearrangement of the solid nickel particles takes place. This stage leads to rapid shrinkage and increase in density and hence strength. Most of the densification in LPS is achieved in this stage. If sufficient amount of liquid is formed with low enough viscosity to flow freely, then the final density at the end of stage I is independent of the starting density, which is determined by laser power and scan speed. The amount of liquid phase formed and the viscosity of the liquid formed depends on the sintering temperature. Higher the sintering temperature, higher is the amount of liquid phase formed with lower the viscosity. But a very high sintering temperature can lead to very high amount of liquid phase with very low viscosity which can result in loss of shape. Particle size of solid phase and rate of heating also determine densification at this stage.

STAGE II : In this stage of LPS, normal densification is accompanied by chemical homogenization between bronze and nickel. Bronze, predominantly copper (90 Wt.%), and nickel homogenize at high temperatures, either by interdiffusion if the homogenization is between solid bronze and solid nickel or by solution-precipitation if the homogenization is between liquid bronze and solid nickel, to form a homogeneous solid solution. In either case, the bronze phase disappears completely leaving behind pores in its place and an expanded solid solution of Cu in Ni. This happens due to a faster diffusion rate of Cu into Ni than that of Ni into Cu, which results in the Kirkendall effect. Therefore, the pores created at this stage are referred to as Kirkendall porosity. Kuczynski has demonstrated the influence of the Kirkendall effect upon sintering in a series of model experiments (10). Therefore, in this stage, normal densification is dominated by the growth or swelling of the part due to Kirkendall porosity.

Detailed investigations of LPS have shown that similar material transport mechanisms prevail during stage I as well as stage II. Therefore, a sharp distinction between these stages is not justified. Whether stage I or stage II predominates the process depends on the particular circumstances. Powder particle size, starting density, sintering temperature, time and rate of heating are most influential in determining this. Effect of some of these variables on LPS will be discussed later with respect to SLS Bronze-Nickel parts. Figure 5 shows the microstructural changes observed with the different stages of LPS and Figure 6 shows the peak broadening occurring due to formation of a homogeneous solid solution of Cu-Ni.

STAGE III : Once homogenization has occurred, only normal shrinkage due to sintering occurs. But now, the sintering occurs in solid state as the temperature is below the solidus of the newly

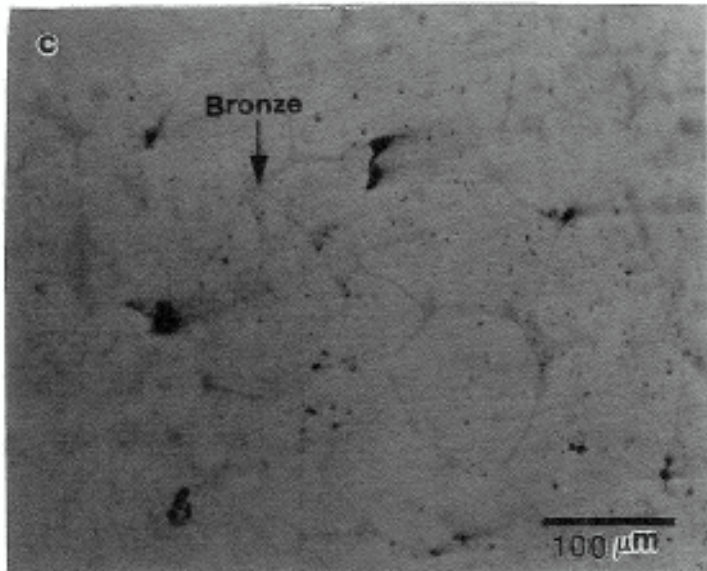
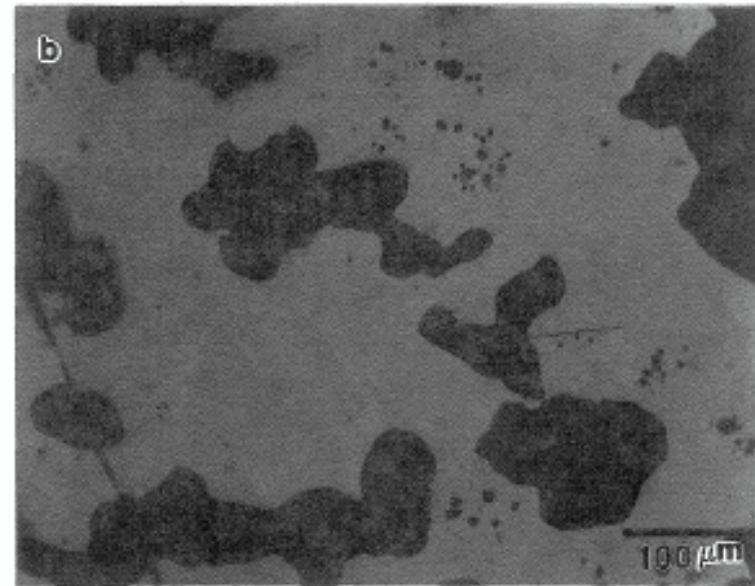
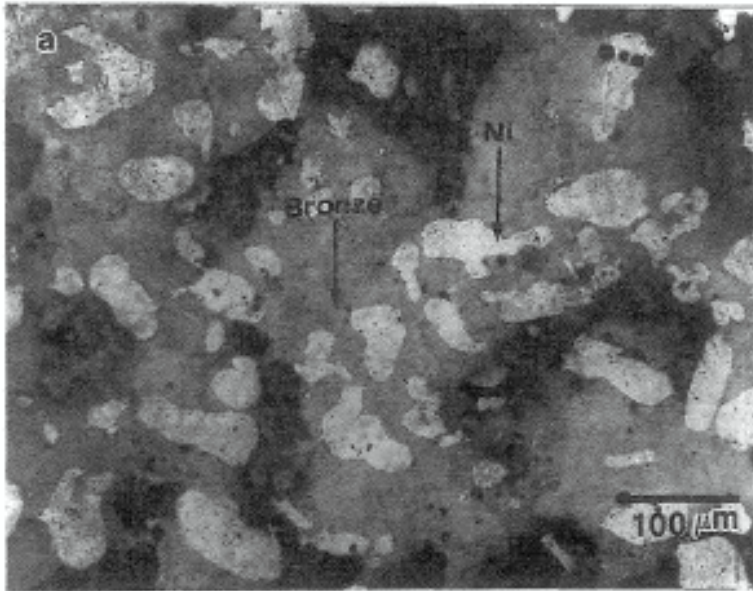


Figure 5. Optical Micrographs of (a) SLS Bronze-Ni Part (56W, 0.3 inch/sec) Showing Bronze and Ni as Separate Phases and High Porosity, (b) Post-SLS Stage II LPS Bronze-Ni Part (56W, 0.3 inch/sec., 950°C, 1 hour) Showing Nearly Homogeneous Phase of Cu-Ni With Some Residual Bronze and High Porosity, (c) Post-SLS Stage I LPS Bronze-Ni Part (56W, 0.3 inch/sec, 1030°C, 1 hour) Showing Nearly Homogeneous Phase of Cu-Ni With Some Residual Bronze and Low Porosity

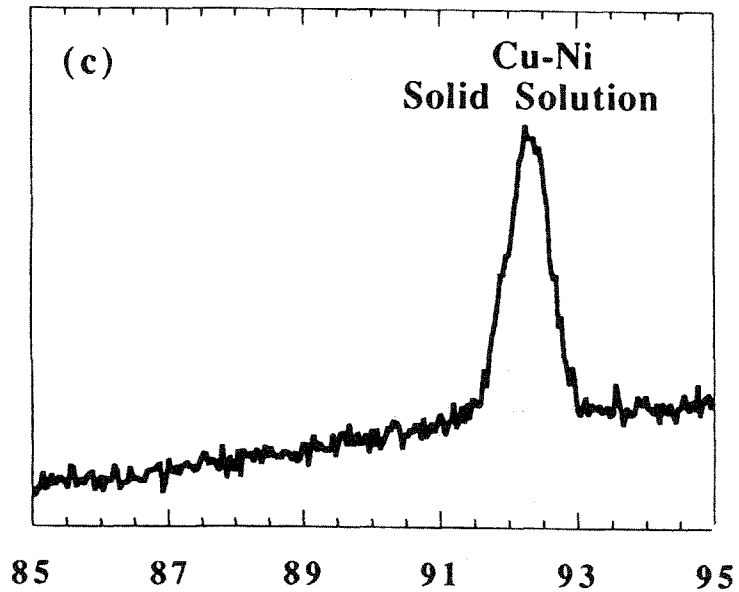
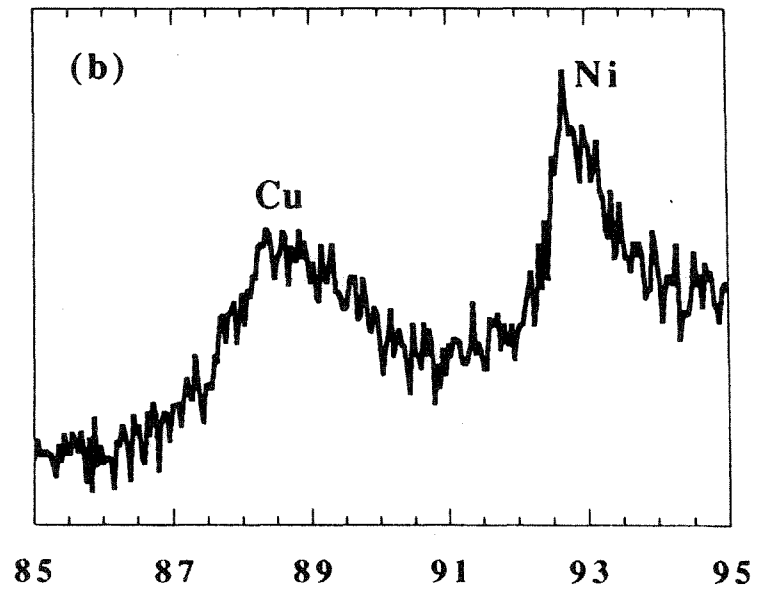
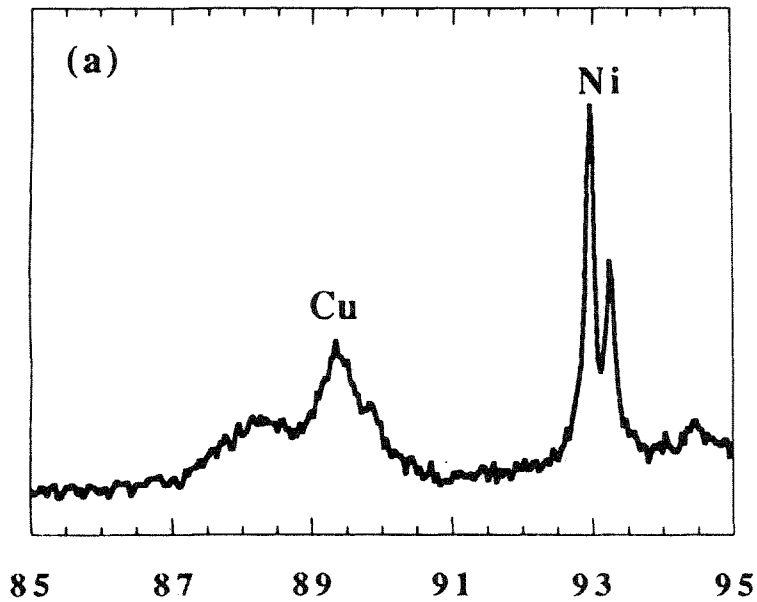


Figure 6. XRD patterns of (311) peaks of Bronze and Nickel showing peak broadening due to homogenization (a) SLS Bronze-Ni Part (56W, 0.3 inch/sec) showing Cu and Ni as separate phases (b) Post-SLS Stage II LPS Bronze-Ni Part (56W, 0.3 inch/sec., 950°C, 1 hour) indicating partial homogenization of Cu and Ni (c) Post-SLS Stage II LPS Bronze-Ni Part (56W, 0.3 inch/sec., 950°C, 6 hour) indicating complete homogenization of Cu and Ni.

formed solid solution of Cu-Ni ($\sim 1100^\circ\text{C}$). Therefore, even for prolonged periods of times, shrinkage or densification during this stage is very small, leaving an overall expansion or shrinkage in the samples, depending on whether first stage or second stage of LPS dominates.

EFFECT OF SINTERING TEMPERATURE AND TIME

As shown in Figures 7, at temperatures below 1000°C the density and strength of SLS parts decrease irrespective of starting densities. The density and strength reach a minimum and then increase slowly to nearly starting densities. At such low temperatures, amount of liquid phase formed is very small with high viscosity which prevents any significant densification normally associated with stage I LPS. Instead, stage II dominates the LPS initially and then stage III continues till the end of the process.

At 1060°C , a temperature well above the liquidus of bronze, bronze is completely in liquid state and has sufficiently low viscosity to allow stage I LPS to dominate. Therefore, the density and hence the strength of the SLS parts increase rapidly at short times of 1 hour. Following this rapid gain in density and strength, there is a slight loss of density and strength due to stage II LPS when the density and strength decrease due to Kirkendall porosity. Some of this loss in density and strength is regained in stage III of LPS due to solid state sintering of Cu-Ni solid solution. At such a high temperature the flow of liquid in stage I is free of any restriction due to low enough viscosity. Therefore, the final density and strength at the end of stage I is independent of starting density and strength. At temperature above 1060°C , the SLS parts exhibited loss of shape even at small times due to significantly lower viscosity of the liquid bronze.

At the liquidus temperature of 1030°C , liquid bronze is more viscous than at 1060°C . Therefore, flow of liquid into pores and rearrangement of solid nickel particles is less dominant. Therefore, the density and strength in stage I at 1030°C is lower than that at 1060°C . In a high-starting-density part, the rigid network of solid nickel particles restrict the flow further and prevent their rearrangement. While in a lower-starting-density part the liquid is more free to flow and rearrange the solid particles. Also, the interdiffusion lengths in a high-starting-density part is smaller, thereby promoting stage II LPS and thus resulting in lower final strengths and density than that for a lower-starting-density part. This effect is more pronounced at 1000°C when the stage II homogenization completely dominates over the stage I densification for a higher-starting-density part. Therefore, at 1000°C , while a high-starting density part exhibits worsening of density and strength, a low-starting-density part exhibits improvements in density and strength.

ANISOTROPIC LINEAR DIMENSIONAL CHANGES

Net volume changes (expansion or shrinkage) of SLS parts during LPS was in accordance with the observed density and strength changes. However, the linear dimensional changes, $\Delta L/L_0$, was not same in all three directions (11). They exhibited some rather interesting trends reflecting the anisotropy in SLS parts.

In general, parts that exhibited swelling or growth during LPS, had a net volume expansion exceeding 10% and was mostly of the order of 15%, resulting in a decrease in fractional density of the order of 8% to 12%, as seen earlier. In accordance with stage II LPS, this decrease was observed over a relatively short period of time followed by a nearly constant density, as would be expected in stage III of LPS. However, the linear dimensional expansion in these parts was anisotropic with least expansion ($\sim 2\%$ - 3%) in the thickness direction, i.e. direction normal to the sintering plane. Most of the expansion (5% - 9%) was confined to the transverse direction (scan direction), Figure 8 (a). A higher degree of sintering along the scan direction, during SLS, results in better density along the transverse direction, thus forming a rigid network of solid nickel and decreasing the interdiffusion lengths. Therefore, stage I LPS is suppressed and stage II LPS dominates along the scan direction yielding a high linear expansion. While a lower degree of

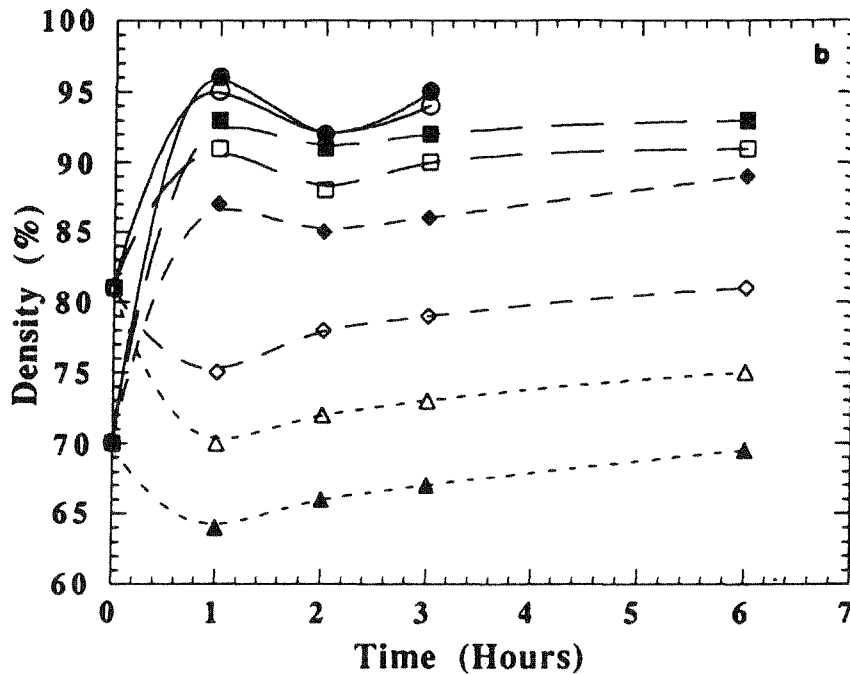
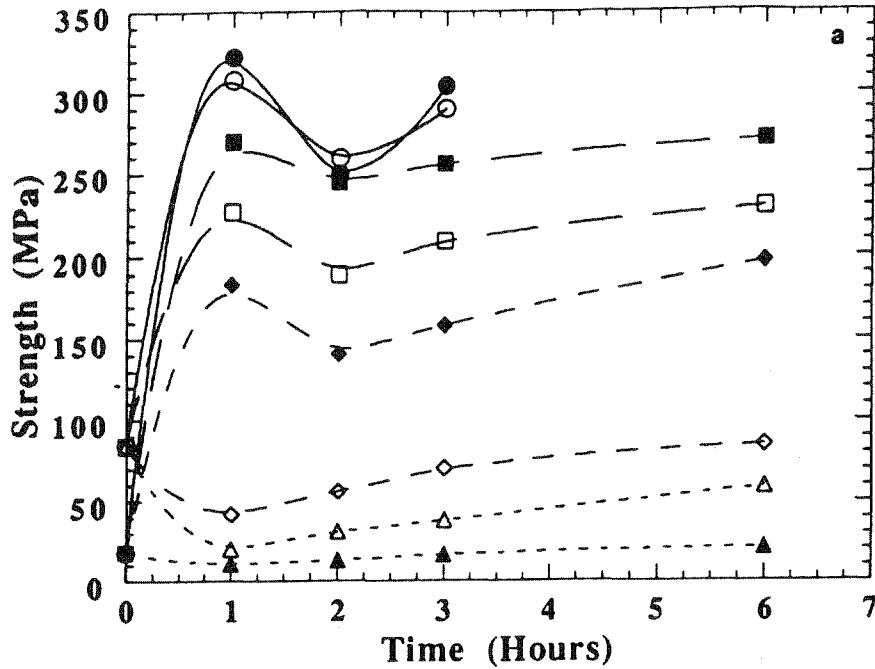
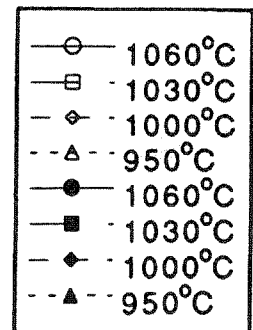


Figure 7.(a) Strength of Post-SLS LPS Bronze-Ni Parts Showing the Effect of LPS Time and Temperature and Starting Density, (b) Fractional Density of Post-SLS LPS Bronze-Ni Parts Showing the Effect of LPS Time and Temperature and Starting density. (Open Symbols - Samples SLS at 0.3 inch/sec. Starting Density 81% and Closed Symbols - Samples SLS at 1.5 inch/sec. Starting Density 70%)



sintering normal to the sintering plane results in poor density between layers leaving a loose network of solid nickel and large interdiffusion lengths. Therefore, stage I LPS is less suppressed and stage II LPS is less dominating between the layers resulting in considerably lower linear expansion. Also, flow of liquid bronze in stage I along the thickness direction is aided by gravity as the samples were post processed with the thickness direction along the direction of gravity.

Like the parts which exhibited growth, the parts exhibiting overall shrinkage or densification also exhibited volume changes according to changes in density, but the linear dimensional changes in the three directions were different. As explained above, since stage I LPS is more dominant along the thickness direction than along the scan direction, higher linear shrinkage was observed in the thickness direction than along the transverse direction. Shrinkage in the longitudinal direction was comparable but higher than along the transverse direction, Figure 8(b).

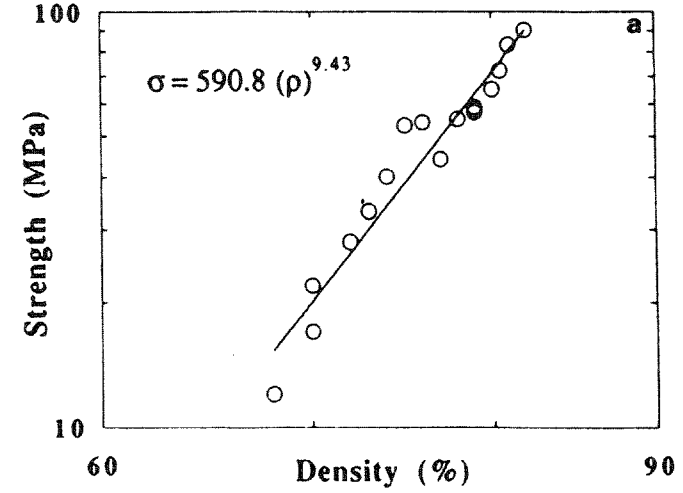
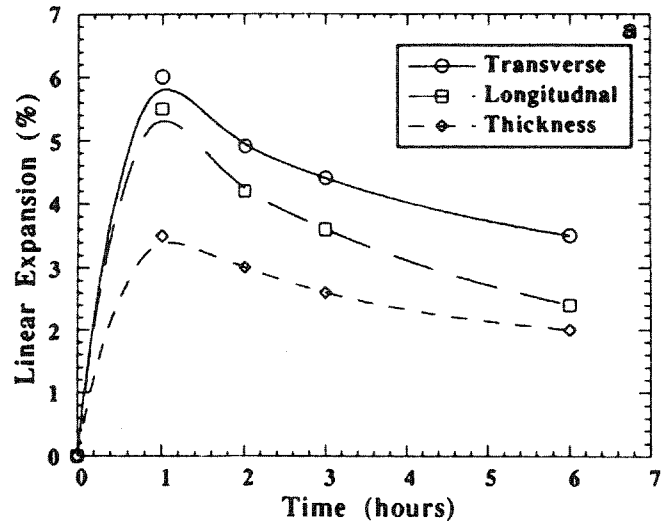
STRENGTH VARIATION WITH DENSITY

As discussed earlier, pores reduce the effective load carrying capacity of a material, thus decreasing the strength of the material. Equation II relates the strength to the fractional density empirically, based on the premise that pores reduce the load bearing capacity of the material. Based on the discussions of results thus far, it can be seen that both the strength as well as density of SLS parts increased with increasing laser power and decreasing scan speed. Therefore, it seems reasonable to relate the strength and density of SLS parts irrespective of the laser power or scan speeds at which they were processed. As shown in Figure 9, a near perfect fit was obtained for the strength and density by relating them using the power law Equation II, with the empirical constants $C\sigma_0$ and m as 590.8 and 9.43 respectively. A high exponent factor, m , of 9.43 indicates large gains in strength for small incremental gains in density. This makes it possible to produce less than fully dense yet structurally sound parts of Bronze-Nickel by direct SLS, without any post-processing. Small incremental gains in density are achievable by increasing the laser power and/or decreasing the scan speed. The "curl" phenomenon associated with high laser power and slow scan speeds can be overcome by using higher bias temperatures in the high-temperature workstation, if light sintering of the powder bed can be avoided or minimised.

Liquid Phase Sintering (LPS) of the SLS Bronze-Ni parts results in an increase or decrease in density and strengths simultaneously as a function of LPS time and temperature, as discussed earlier. Therefore, relating strength with density using the power law form given by Equation II, yields a near perfect fit with the empirical constants $C\sigma_0$ and m as 527.94 and 8.73 respectively, Figure 9(b). From comparison of the empirical constants $C\sigma_0$ and m for SLS Bronze-Nickel parts and for post-SLS LPS Bronze-Nickel parts, it is clear that density and strength vary in a similar way irrespective of the processing. During SLS scan speed and laser power determine the density and strength, while during LPS time and temperature determine the density and strength. SLS laser power is analogous to the LPS temperature as it determines the processing temperature. Similarly, SLS scan speed is analogous to the LPS time as it determines the time of processing. Therefore, by careful manipulation of these four variables it is possible to produce high density, structurally sound parts with no "curl" by direct SLS followed by LPS in very short processing time periods.

CONCLUSIONS

Direct SLS of Bronze-Nickel parts was studied by evaluating the density and strength of the parts as a function of SLS process parameters : laser power, scan speed, scan direction, and layer thickness. Post-SLS processing of the parts was done by Liquid Phase Sintering (LPS) to further enhance the density and strength. LPS of the SLS parts was studied as a function of time and temperature. The relationships between the SLS processing parameters, LPS parameters and the resulting microstructures, density and strengths can be summarized as follows :



202

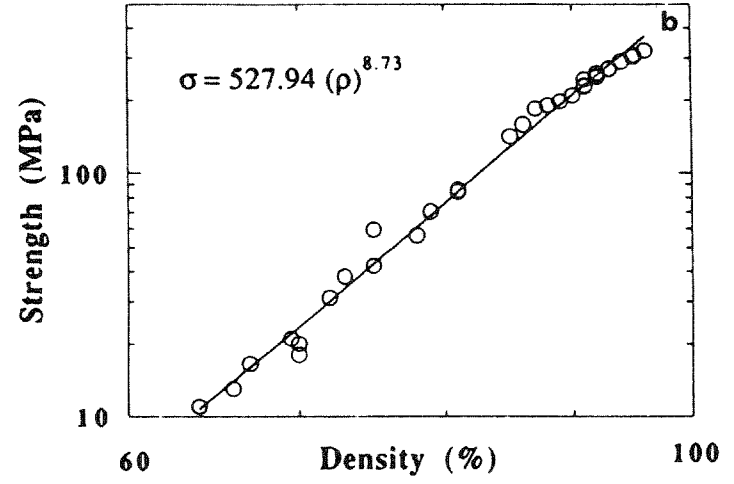
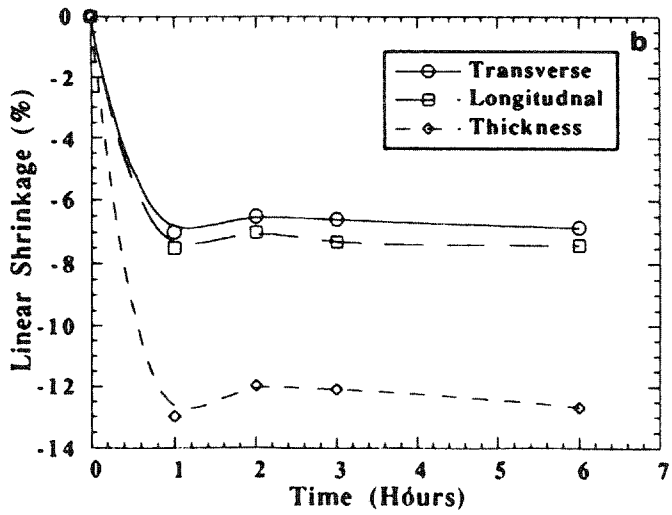


Figure 8. Linear Dimensional Changes Showing Anisotropic Changes (a) Expansion in 56W, 0.3"/sec. SLS Part, LPS at 950°C (b) Shrinkage in 56 W, 1.5"/sec.SLS Sample, LPS at 1030°C.

Figure 9. Strength vs. Density Using Equation II for (a) SLS Bronze-Ni Parts Without Post-SLS Processing (b) Post-SLS LPS Bronze-Ni Parts.

1. Density and strength increase as the layer thickness decreases, scan speed decreases and laser power increases.
2. Scanning in the short transverse direction yielded best results.
3. Strength and density of SLS Bronze-Nickel parts show a very strong power law dependence.
4. LPS of SLS Bronze-Nickel parts improved density and strength at temperatures well above the liquidus temperature of bronze.
5. By LPS at temperatures well below the liquidus temperature of Bronze, density and strength of SLS Bronze-Nickel parts decreased due to Kirkendall porosity resulting from the homogenization of Bronze and Ni.
6. Linear dimensional changes during LPS were anisotropic.
7. Strength and density of post-SLS LPS Bronze-Nickel parts show a similar power law dependence as the SLS Bronze-Nickel parts.

ACKNOWLEDGMENTS

The authors gratefully acknowledge research grants from DTM Corporation, Austin, Texas and NSF Small Grant for Exploratory Research, Grant # DDM-9312603.

REFERENCES

1. G.Zong, Y.Wu, N.Tran, I.Lee, D.L.Bourell, J.J.Beaman, and H.L.Marcus, "Direct Selective Laser Sintering of High Temperature Materials," Proc. of the SFF Symp., Austin, Texas, Aug 3-5, 1992.
2. D.L.Bourell, H.L.Marcus, J.W.Barlow, and J.J.Beaman, "Selective Laser Sintering of Metals and Ceramics," Int. J. Powder Met., 28(4), 369, 1992.
3. S.Das, J.C.McWilliams, Y.Wu, and J.J.Beaman, "Design of a High Temperature Workstation for the Selective Laser Sintering Process," Proc. of the SFF Symp., Austin, Texas, Aug, 1991.
4. J.McWilliams, C.Hysinger, and J.J.Beaman, "Design of a High Temperature Process Chamber for the Selective Laser Sintering Process," Proc. of the SFF Symp., Austin, Texas, Aug 3-5, 1992.
5. ASTM, "Standard Methods of Tension Testing of Metallic Material," 1977 Annual Book of ASTM Standards, Part 6 : Copper and Copper Alloys, ASTM Designation : E8-77, 898-917, 1977..
6. Metals Handbook, Vol.7, 9th Ed., American Society of Metals, Metals Park, OH.
7. J.C.Nelson, and J.W.Barlow, "Relating Operating Parameters Between Selective Laser Sintering Machines which have Different Scanner Geometries and Laser Spot Sizes," Proc. of the SFF Symp., Austin, Texas, Aug 3-5, 1992.
8. R.M.German, "Powder Metallurgy Science," Metal Powder Industries Federation, Princeton, NJ.
9. F.V.Lenel, "Powder Metallurgy - Principles and Applications," Metal Powder Industries Federation, Princeton, NJ.
10. G.C.Kuczynski, "Model Experiments and the Theory of Sintering." From "Sintering - Key Papers," Ed. by S.Somiya and Y.Moriyoshi, Elsevier Applied Science, London and New York.
11. J.C.Nelson, N.K.Vail, M.M.Sun, and J.W.Barlow, "Post-Processing of Selective Laser Sintered Polycarbonate Parts," Proc. of the SFF Symp., Austin, Texas, Aug, 1991.